UC San Diego
UC San Diego Previously Published Works

Title

B3GALT5 knockout alters glycosphingolipid profile and facilitates transition to human naïve pluripotency

Permalink

Journal

Proceedings of the National Academy of Sciences of the United States of America, 117(44)

ISSN

0027-8424

Authors

Lin, Ruey-Jen
Kuo, Ming-Wei
Yang, Bei-Chia
et al.

Publication Date

2020-11-03

DOI

10.1073/pnas.2003155117

Peer reviewed

B3GALT5 knockout alters gycosphingolipid profile and facilitates transition to human naïve pluripotency

Ruey-Jen Lin[a], Ming-Wei Kuo[a], Bei-Chia Yang[a], Hsiu-Hui Tsai[a], Kowa Chen[a], Jing-Rong Huang[a], Yun-Shien Lee[b], Alice L. Yu[a,c,d], and John Yu[a,e,1]

[a]Institute of Stem Cell and Translational Cancer Research, Chang Gung Memorial Hospital at Linkou, 333 Taoyuan, Taiwan; [b]Department of Biotechnology, Ming-Chuan University, 333 Taoyuan, Taiwan; [c]Genomics Research Center, Academia Sinica, 115 Taipei, Taiwan; [d]Division of Hematology and Oncology, Department of Pediatrics, University of California, San Diego, CA 92123; and [e]Institute of Cellular and Organismic Biology, Academia Sinica, 115 Taipei, Taiwan

Conversion of human pluripotent stem cells from primed to naïve state is accompanied by altered transcriptome and methylome, but glycosphingolipid (GSL) profiles in naïve human embryonic stem cells (hESCs) have not been systematically characterized. Here we showed a switch from globo-(SSEA-3, SSEA-4, and Globo H) and lacto-series (fucosyl-Lc4Cer) to neolacto-series GSLs (SSEA-1 and H type 2 antigen), along with marked down-regulation of β-1,3-galactosyltransferase (B3GALT5) upon conversion to naïve state. CRISPR/Cas9-generated *B3GALT5*-knockout (KO) hESCs displayed an altered GSL profile, increased cloning efficiency and intracellular Ca^{2+}, reminiscent of the naïve state, while retaining differentiation ability. The altered GSLs could be rescued through overexpression of B3GALT5. *B3GALT5*-KO cells cultured with 2iLAF exhibited naïve-like transcriptome, global DNA hypomethylation, and X-chromosome reactivation. In addition, *B3GALT5*-KO rendered hESCs more resistant to calcium chelator in blocking entry into naïve state. Thus, loss of B3GALT5 induces a distinctive state of hESCs displaying unique GSL profiling with expression of neolacto-glycans, increased Ca^{2+}, and conducive for transition to naïve pluripotency.

B3GALT5 | human embryonic stem cells | glycosphingolipids | intracellular calcium | naïve pluripotency

It has been suggested that conventional mouse and human embryonic stem cells (hESCs) exist in two developmental stages, the naïve and primed states, which recapitulate properties of pre- and postimplantation blastocyst stages, respectively (1, 2). Although both naïve and primed ESCs express OCT4, NANOG, and SOX2, can self-renew indefinitely, and differentiate into three germ cells, they are morphologically, molecularly, and functionally distinct. Naïve-state cells harbor features of ESCs with specific transcriptome, DNA hypomethylation, and X chromosome reactivation, similar to human preimplantation embryos (3–6). They require different extrinsic signals for the maintenance of self-renewal and pluripotency (7).

Recently, multiple methods for conversion of primed hESCs to naïve-like phenotype have been reported (8–11). The hESCs cultured in 5iLAF medium composed of five inhibitors (MEK, GSK-3, Src, B-Raf, and ROCK inhibitors), leukemia inhibitory factor (LIF), activin A, and FGF2 (8), are considered to be in the naïve state. These cells display features distinctly different from primed hESCs and resemble early-stage human epiblasts (4, 5, 12). Mouse ESCs, which are naïve pluripotent stem cells, express stage-specific embryonic antigen-1 (SSEA-1) (13), whereas hESCs, which are primed pluripotent stem cells, express SSEA-3, SSEA-4, TRA-1-60, and TRA-1-81 (6, 7). Whether differences in glycan markers in mouse and human ESCs reflect differences in the development stages or species origins has not been resolved. In particular, the dynamic changes in glycosphingolipid (GSL) expression during primed-to-naïve state conversion in hESCs remain to be delineated.

GSLs are omnipresent surface components of animal cells and function as modulators in cell–cell interactions, cell-extracellular matrix interactions, and ligand-receptor interactions, including FGF, Wnt, Hh, and BMP (14, 15). Emerging evidence suggests that GSL profiles are cell- or tissue-specific and developmentally regulated. Antibodies against several GSLs designated as SSEAs have been widely used to characterize ESCs. However, due to cross-reactivities of antibodies with many glycans (16–18), systematic mass spectrometry (MS) analysis is often employed to decipher the GSL profiles (19). With the combined use of antibodies and matrix-assisted laser desorption/ionization (MALDI)-MS and MS/MS analyses, we previously showed that in addition to the well-known hESC-specific markers, SSEA-3 and SSEA-4, several previously undisclosed globo- (Gb4Cer, Globo H, and disialyl-Gb5Cer) and lacto-series GSLs (Lc4Cer and fucosyl-Lc4Cer) are also expressed in undifferentiated hESCs (18–20). Upon differentiation, the GSLs profiles switched from globo- and lacto- to ganglio-series. Furthermore, the GSL pattern shifted to primarily ganglio-series dominated by GD3 during differentiation into neural progenitors, but shifted to prominent expression of Gb4Cer during endodermal differentiation (18, 20). Such alterations of specific GSLs were accompanied by changes in glycosyltransferases in their biosynthetic pathways (18, 20). It was reported that hESCs in 5iLAF culture did not stain with SSEA-4 antibody but displayed naïve-like features (5). However, during

Significance

These studies provide systematically characterized glycosphingolipid (GSL) profiles and expression level of glycosyltransferase upon the conversion of human ESCs from primed to naïve state. We identify a switch of GSL profile from globo- and lacto-series to neolacto-series GSLs, accompanied by the downregulation of β-1,3-galactosyltransferase (B3GALT5) during the pluripotency transition. The CRISPR/Cas9-generated *B3GALT5* knockout increases the level of intracellular Ca^{2+}, resulting in an intermediate state of pluripotency, which facilitates the primed-to-naïve-state transition in human ESCs. In addition, the altered GSL could be rescued through overexpression of B3GALT5. Thus, our results provide a new perspective in the understanding of human pluripotency transition from primed to naïve state, which can be facilitated by changing the expression of single glycosyltransferase, B3GALT5.

DEVELOPMENTAL BIOLOGY

conversion from primed to naïve pluripotency, it remains to be delineated whether there are systematic alterations in glycan profile and whether these alterations are accompanied by specific changes in glycosyltransferases.

In this study, we examined the dynamic changes in GSL profile and glycosyltransferases in primed and naïve state of hESCs by combined use of mAbs and MS analysis. We demonstrated that loss of B3GALT5 (β-1,3-galactosyltransferase) with consequent shifts from globo- and lacto-series to neolacto-series glycans in hESCs and increased intracellular calcium facilitated the transition to naïve pluripotency.

Results

GSL Profiling in Naïve and Primed hESCs. Primed hESCs reportedly convert to the naïve state (5, 8, 21) under 5iLAF conditions, which was originally designed by Theunissen et al. (8). This 5iLAF consists of medium supplemented with LIF, activin A, and FGF2, plus five inhibitors for ERK, GSK3, BRAF, SRC, and ROCK. As shown in *SI Appendix*, Fig. S1 *A and B*, 5iLAF-cultured H9 hESCs grew in small, round colonies similar to naïve mouse ESCs and expressed unique naïve-specific markers (KLF4, TFCP2L1, STELLA, TBX3, and TFE3). In contrast, pluripotent (NANOG, OCT3/4, and SOX2) and surface markers (TRA-1-60 and TRA-1-81) were expressed in both naïve- and primed-state hESCs (*SI Appendix*, Fig. S1*C*), as reported previously (3).

In immunostaining studies of GSL profile, SSEA-3, SSEA-4, Globo H, and fucosyl-Lc4Cer (H type 1 glycan or SSEA-5) were highly expressed in primed-state hESCs (Fig. 1*A*). In contrast, these GSLs disappeared almost completely after conversion of cells to the naïve state in 5iLAF culture (Fig. 1*A*). Considering the cross-reactivity of glycan antibodies (16–18), we used MALDI-MS analysis for GSL profiling of hESCs. MALDI-MS signals were observed in primed cells for Fuc1Hex4HexNAc1Cer (Globo H) at m/z 1,838 to 1,950, Hex4HexNAc1Cer (SSEA-3) at m/z 1,664 to 1,776, Neu5AC1Hex4HexNAcCer (SSEA-4) at m/z 2,025 to 2,137, and Fucα2Galβ3GlcNAcβ3Galβ4Glcβ1Cer (fucosyl-Lc4Cer) at m/z 1,634 to 1,746, suggesting that these globo- and lacto-series GSLs were indeed expressed in the primed but not naïve state (Fig. 1*B*). Thus, these results validate the observations from immunostaining studies. In addition, Gb3Cer (the precursor of globo-series GSLs) was detected in both primed- and naïve-state hESCs (Fig. 1*B*). However, signals for Gb4/Lc4Cer and LacCer were weaker in the naïve than the primed state (Fig. 1*B*).

Interestingly, immunostaining with antibodies against the neolacto-carbohydrate chains SSEA-1 (CD15) and blood group H type 2 antigen (H type 2 or CD173) was strongly positive in naïve- but not primed-state hESCs (Fig. 1*A*). However, these glycans were not detected by MALDI-MS analysis of GSL extracts (Fig. 1*B*) in either primed or naïve hESCs, suggesting that the neolacto core chains are most likely present as glycoconjugates in glycoproteins in naïve hESCs.

Expression of GSL-Related Glycosyltransferases in Naïve and Primed hESCs. To investigate the mechanism of GSL changes in naïve hESCs, the expression of glycosyltransferases involved in GSL biosynthetic pathways (Fig. 1*D*) was analyzed by qRT-PCR. In naïve hESCs, *B3GALT5*, which is involved in the synthesis of both globo- (SSEA-3 [Gb5Cer]) and lacto-series (Lc4Cer) GSLs, was down-regulated to 23% of the primed-state level, thus contributing to the reductions in SSEA-3 and Lc4Cer in naïve cells. The levels of two fucosyltransferases, *FUT1* and *FUT2*, which catalyze the synthesis of fucosyl-Gb5Cer (Globo H) and fucosyl-Lc4Cer, decreased in naïve-state cells to 43% and 36%, respectively, of primed-state levels. The expressions of *ST3GAL2* (ST3 β-galactoside α-2,3-sialyltransferase 2), which is responsible for sialylation of Gb5Cer to generate SSEA-4, and of *A4GALT* (Gb3 synthase) decreased to 67% and 66%, respectively, of primed-state levels (Fig. 1*C*). These changes in glycosyltransferase

expression may explain the down-regulation of globo-series (SSEA-3, SSEA-4, and Globo H) and lacto-series (fucosyl-Lc4Cer) GSLs, when hESCs are converted to the naïve state.

Furthermore, single-cell RNA-sequencing (RNA-seq) analysis of the E-MTAB-6819 (22) online dataset revealed no detectable *B3GALT5* in naïve state, as compared to primed state (*SI Appendix*, Fig. S2*A*). We also validated the down-regulation of *B3GALT5* in HUES6 cells, and four datasets (8, 10, 23, 24) of microarray or next-generation sequencing for hESC lines H1, H9, WIBR2, and WIBR3 when cultured in naïve conditions (*SI Appendix*, Fig. S2 *B and C*). These results suggested that B3GALT5, which was involved in biosynthesis pathways for globo- and lacto-series GSLs and markedly down-regulated in naïve hESCs, may play key roles in the unique changes of GSL profiles upon primed to naïve conversion.

Effect of *B3GALT5* Knockout in hESCs. To further address the role of B3GALT5 in human naïve pluripotency, we generated homozygous deletion of *B3GALT5* in H9 hESCs by genomic editing with a CRISPR/Cas9 method. The lack of off-targeting effects in *B3GALT5* knockout (KO) cells was validated as described in *Materials and Methods*. In addition, the sequencing data verified double-mutation alleles (16-bp and 11-bp deletion) near the single-guide RNA (sgRNA) site in exon 4 of *B3GALT5* (Fig. 2*A*), thus confirming homologous KO in these cells. Next, to validate the loss of B3GALT5 function, KO cells were shown to be devoid of expression of SSEA-3, SSEA-4, fucosyl-Lc4Cer, and Globo H by immunostaining (Fig. 2*B*) and MALDI-MS analysis (*SI Appendix*, Fig. S3). Furthermore, overexpression of *B3GALT5* in KO cells rescued the expression of these GSLs (Fig. 2*C*). Collectively, these results indicate that B3GALT5 is the key glycosyltransferase responsible for the biosynthesis of SSEA-3, SSEA-4, fucosyl-Lc4Cer, and Globo H.

B3GALT5 reportedly is also responsible for biosynthesis of type 1 chain structure (Galβ1–3GlcNAc) (19, 25). Consequently, the expression of stem markers, TRA-1-60 and TRA-1-81, which have a type 1 chain epitope (26), also disappeared in *B3GALT5*-KO cells (Fig. 2*B*). On the other hand, we observed high expression of the neolacto-series SSEA-1 and H type 2 antigen in *B3GALT5*-KO hESCs (Fig. 2*B*). But, in contrast to the decreases in expression of glycosyltransferase genes related to GSLs on conversion from the primed to naïve state of H9 cells (Fig. 1*C*), *B3GALT5*-KO and WT H9 cells did not exhibit significant differences in expression of glycosyltransferases, such as *B4GALT1*, -3, and -4, or *Fut4* and -9 (*SI Appendix*, Fig. S4), implying that high expression of SSEA-1 and H type 2 antigen was not due to the changes of these glycosyltransferases. These findings indicate that specific KO of *B3GALT5* blocked the synthesis of not only globo- and lacto- series GSLs, but also type 1 chain epitope (e.g., TRA-1-60 and TRA-1-81), while increasing the synthesis of neolacto-series glycans (SSEA-1 and H type 2 antigen).

B3GALT5 KO Facilitates the Generation of Naïve Pluripotency. Moreover, we found no substantial differences in the morphology of *B3GALT5*-KO and WT hESCs or in the expression of the pluripotency stem cell markers NANOG, OCT3/4, and SOX2 (*SI Appendix*, Fig. S5*A*). However, *B3GALT5*-KO hESCs had a significant 1.6-fold increase in cloning efficiency at low seeding density (Fig. 2*D*), suggesting that *B3GALT5*-KO cells are more resistant to cell death associated with single-cell suspension. *B3GALT5*-KO cells also differentiated into three germ lineages in vitro. We observed robust expression of lineage markers, as shown by immunostaining for SOX1 and b3-tubulin for mature neurons (ectoderm), a-Actinin, NKX2.5, and TNNT2 for cardiomyocytes (mesoderm), and HNF-4a and albumin for hepatocytes (endoderm) (Fig. 2*E*). Moreover, KO cells were capable of generating teratomas containing all three germ layers in immunodeficient mice (Fig. 2*F*). These results indicate that KO of *B3GALT5* did not
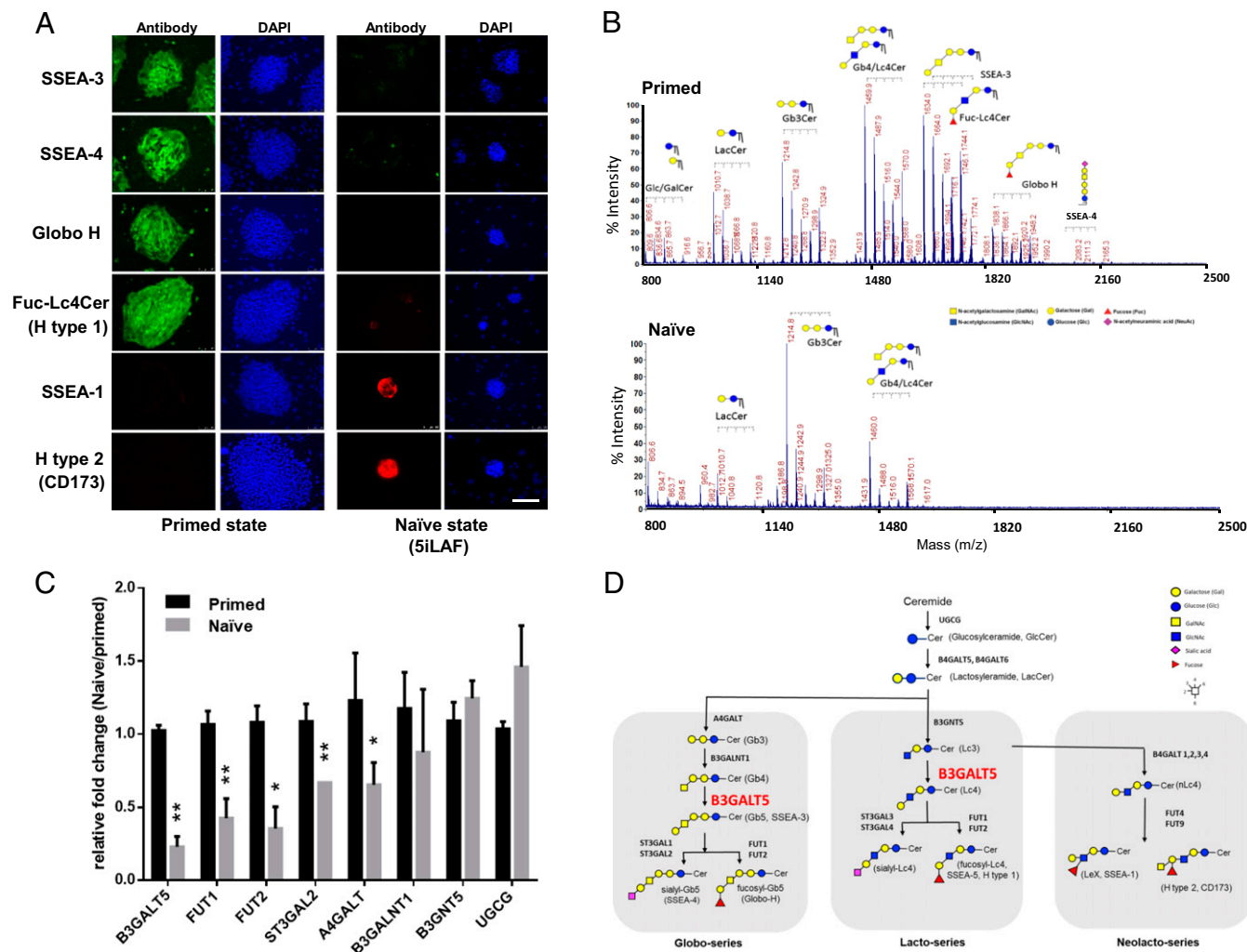
Fig. 1. Characterization of primed- and naïve-state hESCs: GSL profiles and mRNA expression levels of glycosyltransferases. (*A*) Human primed and naïve (cultured in 5iLAF) H9 hESCs were examined. The expression of SSEA-3, SSEA-4, Fuc-Lc4Cer (fucosyl-Lc4Cer), and Globo H was not observed in naïve hESCs by immunofluorescence staining. GSL-specific antibodies are stained green or red, and nuclei are stained blue with DAPI. (Scale bar, 200 μm.) (*B*) MALDI-MS profiles of GSLs from primed and naïve state hESCs. Glycan compositions of main peaks are annotated. The transition from primed to naïve state was accompanied by decreases in SSEA-3, Globo H, SSEA-4, and Fuc-Lc4Cer. (*C*) Expression of GSL-related glycosyltransferase genes was analyzed by qRT-PCR. Relative quantities are presented as the ratios of naïve/primed hESCs. Results are shown as mean ± SEM of three independent experiments. *$P < 0.05$, **$P < 0.01$; two-tailed *t* test. (*D*) The biosynthetic pathway of GSL. Each experiment replicates three times.

affect the maintenance of pluripotency markers, nor alter the in vitro and in vivo capacity of cells to differentiate.

Furthermore, similar to WT hESCs, these *B3GALT5*-KO cells could be converted to the naïve state under 5iLAF culture conditions displaying the characteristic dome-like colony morphology (Fig. 3*A*). It was shown previously that 2i/LIF medium, which contained LIF and two inhibitors for ERK (PD0325901) and GSK3 (CHIR99021) for mouse ESCs, was inadequate for converting hESCs into the naïve state (27). On the other hand, for studies of hESCs using 5iLAF medium to convert primed to naïve state in hESCs (5, 8, 21, 28), activin A and FGF2 were added to the formulation, presumably because of the enhancement of the kinetics for naïve conversion through the reduction of lineage differentiation (8). Therefore, in order to compare the conversion of WT- and *B3GALT5* KO-hESCs to naïve state, we employed the use of 2iLAF, which consisted of medium supplemented with LIF, activin A, and FGF2, but contained only two inhibitors for ERK and GSK3. Unexpectedly, when cultured in this 2iLAF medium, *B3GALT5*-KO cells displayed the characteristic naïve-specific dome-like colony morphology similar to

those cultured in 5iLAF media, whereas WT hESCs failed to do so in the same medium (Fig. 3*A*). *B3GALT5*-KO cells cultured in 2iLAF medium continued to express pluripotency markers (NANOG, OCT3/4, and SOX2) and display naïve-specific markers (KLF4, TFCP2L1, STELLA, TBX3, and TFE3) (Fig. 3*B*). The presence of these markers associated with primed and naïve pluripotency was also confirmed by qRT-PCR (*SI Appendix*, Fig. S5*B*). Of note, WT cells cultured in 2iLAF displayed comparable down-regulation of primed markers (DUSP6, ZIC2), and up-regulation of four of six naïve markers (KLF4, KLF2, TBX3, DNMT3L), albeit at lower levels than those in naïve WT+5iLAF and KO+2iLAF cells (*SI Appendix*, Fig. S5*B*). Similar findings were observed when another hESC, HUES6 cells, were treated with 2iLAF (*SI Appendix*, Fig. S5*C*). These results thus suggest that the culture of WT-hESCs in 2iLAF could only partially convert hESCs toward naïve state, but not completely.

In addition, the genome-wide assessment of the effects of B3GALT5 deficiency on transcription in naïve and primed hESCs was performed with RNA-seq. As shown in Fig. 3*C*,
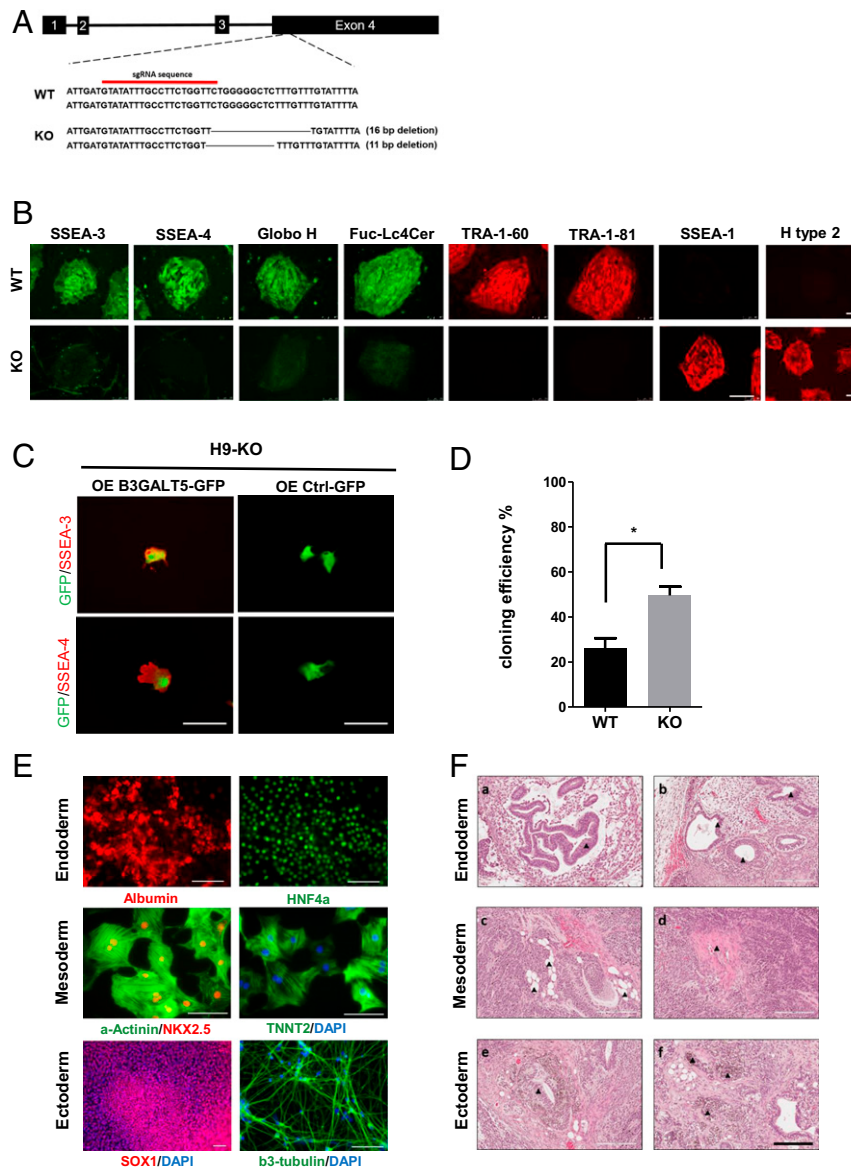
Fig. 2. Characterization of *B3GALT5*-KO hESCs. (*A*) CRISPR-mediated disruption of the *B3GALT5* gene in H9 hESCs. The sgRNA targeting exon4 of *B3GALT5* is illustrated. DNA sequencing results of *B3GALT5*-WT and KO H9 cells show double mutation alleles (16-bp and 11-bp deletion) in KO cells. (*B*) Immunofluorescence staining for the expression of SSEA-3, SSEA-4, Fuc-Lc4Cer (fucosyl-Lc4Cer), Globo H, TRA-1-60, TRA-1-81, SSEA-1, and H type 2 (CD173, blood group H type 2 antigen) in KO and WT cells of H9. (Scale bars, 200 μm.) (*C*) Immunofluorescence staining for the expression of SSEA-3 and SSEA-4 in KO cells of H9, as compared with the control cells, after rescue via overexpression (OE) of B3GALT5 (OE B3GALT5-GFP) and vector only (OE Ctrl-GFP) in the cells. GFP⁺ cells indicate Ctrl-GFP-OE or B3GALT5-GFP-OE cells. (Scale bars, 100 μm.) (*D*) KO of *B3GALT5* increases the cloning efficiency of hESCs at low seeding density. Data represent mean ± SEM. (*$P < 0.05$; two-tailed *t* test; $n = 3$ biologically independent experiments). (*E*) KO hESCs can differentiate into ectoderm, mesoderm, and endoderm cells in vitro. Lineage markers include SOX1 and b3-tubulin for mature neurons (ectoderm), a-Actinin, NKX2.5, and TNNT2 for cardiomyocytes (mesoderm), and albumin and HNF-4a for hepatocytes (endoderm). (Scale bars, 100 μm.) (*F*) Teratoma formation from KO hESCs. KO hESCs can differentiate into ectoderm, mesoderm, and endoderm cells in vivo. H&E-stained teratomas showed multiple differentiated tissues including cells of endoderm (*a* and *b*: gut tube-like structures), mesoderm (*c*: adipose-like tissue, *d*: smooth muscle-like tissue), and ectoderm (*e*: neuronal rosette-like structures, *f*: melanocytes). Referenced structures are indicated by arrowheads. (Scale bar, 200 μm.)

principal component analysis (PCA) of these samples showed that the major transcriptional changes along principal component 1 (PC1, 75.7% total variability) clearly separated all primed cells (WT and KO) from all naïve cells (WT+5iLAF and KO+2iLAF). In contrast, WT+2iLAF clustered closer to the primed cells along the PC1, but also set itself apart from both primed and naïve cells. Furthermore, statistical analysis comparing the primed cells (WT) with the naïve-converted cells (WT+5iLAF, KO+2iLAF) revealed differential expression of 1,192 genes (false-discovery rate < 0.05, |log 2 fold-change| > 2).

Clustering analysis based on the differentially expressed genes (DEGs) also clearly showed two distinctive groups with similar gene-expression pattern between WT and KO cells, as well as between WT+5iLAF and KO+2iLAF cells (Fig. 3*D*). On the other hand, the gene profiling in WT+2iLAF cells was closer to the primed cells, albeit with some disparity. These findings further support that KO cells in 2iLAF, but not WT+2iLAF, were converted to a naïve state similar to WT cells in 5iLAF culture.

To further substantiate that *B3GALT5*-KO cells cultured in 2iLAF were in a naïve state, hallmarks of naïve hESCs, such as X
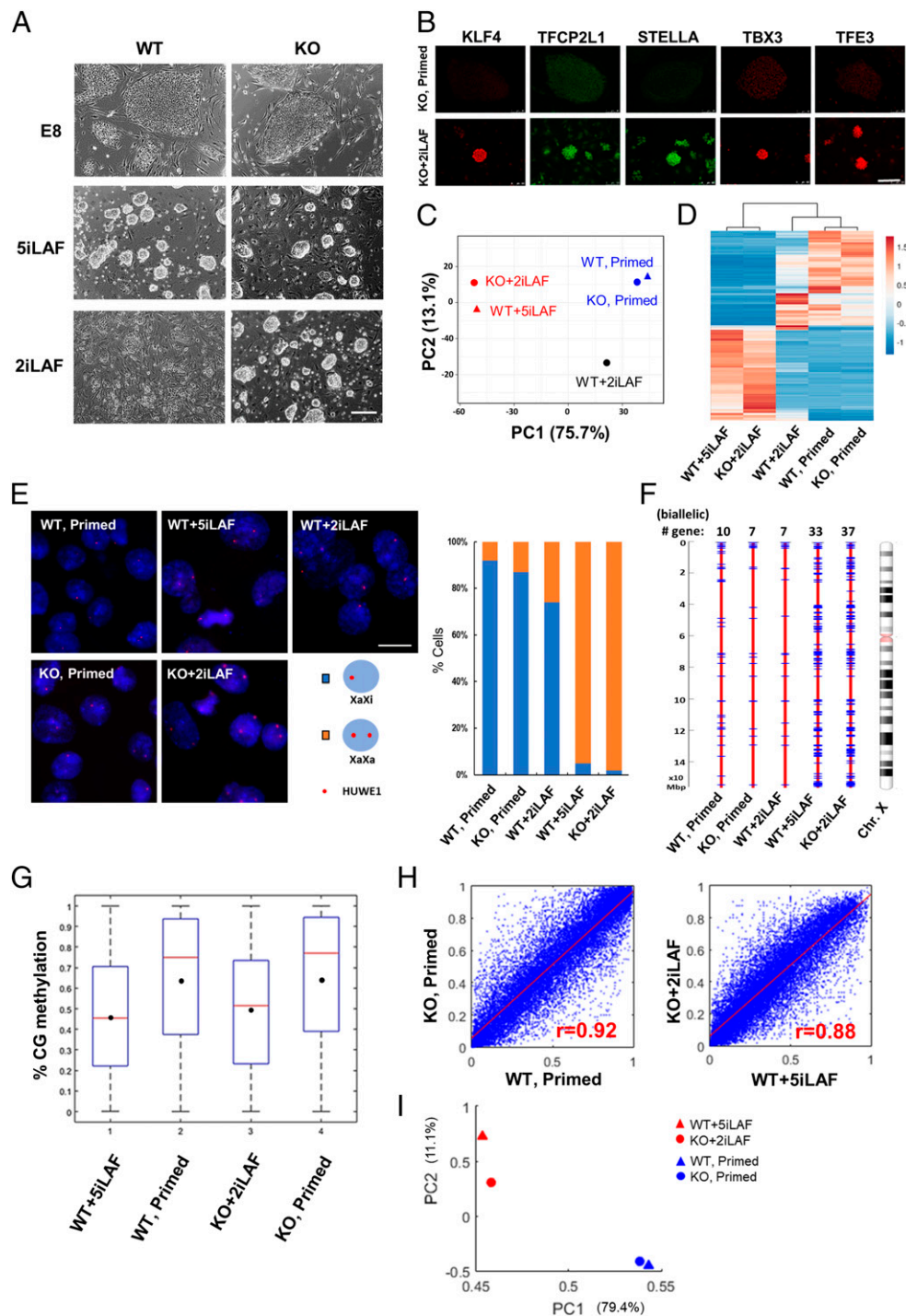
Fig. 3. *B3GALT5* KO promotes the generation of naïve state. (*A*) Representative morphology of WT and KO cells of H9 cultured in the indicated E8, 2iLAF, or 5iLAF medium. The WT cells in 5iLAF (WT+5iLAF) and KO cells in 5iLAF (KO+5iLAF) or 2iLAF (KO+2iLAF) have naïve-specific dome-like morphology. (Scale bar, 200 μm.) (*B*) Immunofluorescence staining for expression of naïve-specific markers (KLF4, TFCP2L1, STELLA, TBX3, and TFE3) in KO and KO+2iLAF cells of H9. (Scale bars, 200 μm.) (*C*) PCA of RNA-seq data for the indicated samples. (*D*) Heat map and the unsupervised hierarchical clustering of 1,192 DEGs for genome-wide comparison of the primed and naïve states. (*E*) Representative RNA-FISH images detecting HUWE1 nascent transcripts (red) in DAPI-stained nuclei (blue) for the indicated cells. Mono- or biallelic HUWE1 pattern is depicted in the cartoon (*Lower Right*) and quantified in the *Left*. (Scale bar, 20 μm.) (*F*) Schematic drawing of X chromosomes that summarize the results of an allelic analysis of RNA-seq data for the indicated cell types. Informative SNPs within X-linked genes of the H9 (30) were used to classify expression as monoallelic or biallelic. The biallelic SNPs are marked as blue lines in each column of the indicated cell types and the number of biallelic genes is shown on the top of each column. (*G–I*) DNA methylation patterns in primed and naïve hESCs by whole-genome bisulfite sequencing. (*G*) Box-plot of global CG methylation levels in primed (WT and KO) and naïve H9 (WT+5iLAF and KO+2iLAF). Black circles indicate mean value. Hypermethylation is observed in WT and KO cells as compared to WT+5iLAF and KO+2iLAF cells. (*H*) Correlation plots of the percentage of CG methylation in WT and KO cells (*Left*) and in WT+5iLAF and KO+2iLAF cells (*Right*). (*I*) The PCA analysis of DNA methylation data for primed (blue) and naïve cells (red). Percentage labels on each axis denote the variance described by that PC. There is clear separation of cells with primed status (WT, KO) and naïve status (WT+5iLAF and KO+2iLAF).

chromosome reactivation and global DNA hypomethylation (5, 6, 29), were assessed. We performed RNA-FISH for nascent transcripts of the X-lined gene, HUWE1 (Fig. 3E, red) (29) to confirm X chromosome reactivation in naïve state. As shown in Fig. 3E, both primed WT and KO hESCs displayed monoallelic expression of HUWE1, consistent with X chromosome-inactivated (XaXi). In contrast, biallelic expression supporting X chromosome reactivation (XaXa) was observed in WT naïve cells treated with 5iLAF and in KO cells cultured in 2iLAF. It is noteworthy that WT cells in 2iLAF displayed only 26% of XaXa, supporting that 2iLAF medium is not sufficient to drive complete X chromosome reactivation. Furthermore, we also examined our RNA-seq data to determine the allele-specific expression of X-linked genes and classified informative transcripts as monoallelic or biallelic, using heterozygous SNPs on the X chromosome of H9 cells (30). This analysis revealed that there was a significantly greater number of X-linked genes with biallelic expression in WT cells treated with 5iLAF and in KO cells cultured in 2iLAF (Fig. 3F) than WT, KO, and WT in 2iLAF cells; these findings further supported that X chromosome reactivation occurred primarily in these naïve cells.

Next, changes in DNA methylation in *B3GALT5*-KO and WT hESCs cultured in 2iLAF and 5iLAF, respectively, were assessed by whole-genome bisulfite sequencing. Conversion of primed hESCs to the naïve state in 5iLAF culture resulted in a global decrease in DNA methylation from 75.0 to 45.5% (Fig. 3G). Similarly, in *B3GALT5*-KO cells cultured in 2iLAF, DNA methylation was globally reduced from 77.1 to 51.5%. Also, the level of methylation of DNA CpG sites in *B3GALT5*-KO cultured in 2iLAF correlated strongly with that in WT hESCs cultured in 5iLAF, which exhibited naïve features ($r = 0.88$), whereas the level in *B3GALT5*-KO cultured under primed conditions correlated with that in WT cells cultured under similar conditions ($r = 0.92$) (Fig. 3H). Finally, PCA analysis confirmed the differences in DNA methylome between naïve and primed hESCs. Methylation data for naïve-state cells (*B3GALT5*-KO cells cultured in 2iLAF and WT hESCs in 5iLAF) clustered together, but was clearly separated from data for primed cells (WT and *B3GALT5*-KO cells) (Fig. 3I).

Additionally, to confirm the impacts of B3GALT5 on GSL profiling of hESCs and to avoid the cell line bias, we generated
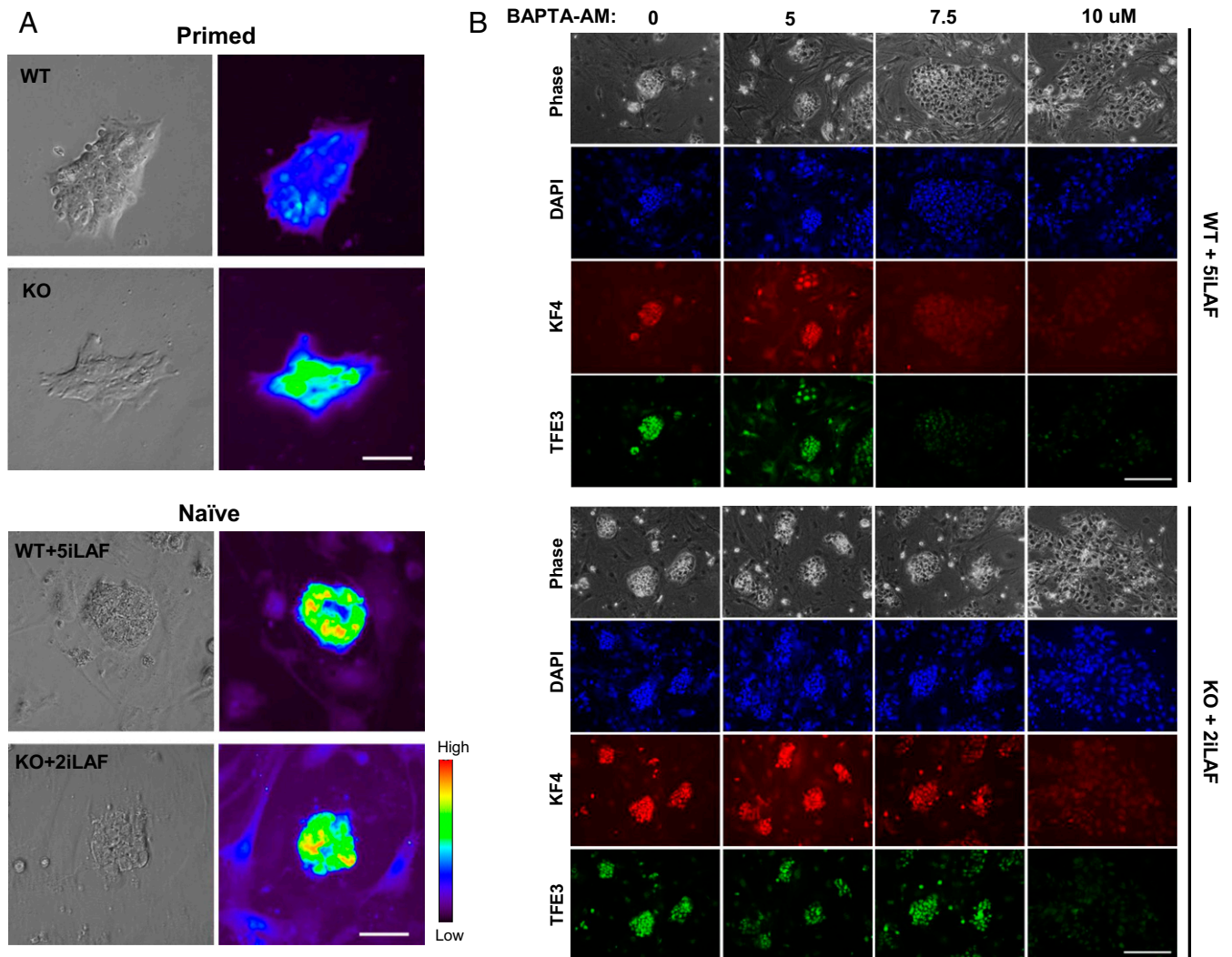
Fig. 4. *B3GALT5* KO leads to an increase in intracellular Ca^{2+} required for naïve pluripotency. (A) Intracellular Ca^{2+} was visualized in H9 primed hESCs and naïve cells generated from WT+5iLAF and KO+2iLAF cells at 8 d. Cells were loaded with the cell-permeable fluorescent calcium indicator Fluo-4 AM. Ca^{2+} imaging was conducted using a fluorescent microscope. Both phase-contrast images and the fluorescence intensities of the cells with Fluo-4 AM displayed in spectrum are shown. Color-coded bar for intensity calibration is shown on the right. (Scale bars, 50 μm.) (B) Representative pictures for morphology and naïve makers (KLF4 and TFE3) of the WT and KO cells in the naïve culture condition (with 5iLAF and 2iLAF, respectively, for 8 d) and with or without BAPTA-AM (0 to 10 μM). Specific antibodies were stained green or red, and nuclei were stained blue with DAPI. (Scale bars, 100 μm.)

B3GALT5-KO hESCs in another hESC line, HUES6, using the same gene-editing strategy described above. Alterations in GSL expression, reminiscent of the naïve-like features in the 2iLAF condition, similar to *B3GALT5*-KO of H9 hESCs, were also observed in HUES6 KO cells (*SI Appendix*, Fig. S6). Moreover, to explicitly rule out the potential effects of gene KO on chromosomal abnormalities, we examined the karyotypes of the KO cells cultured in primed and naïve conditions. These cells were karyotypically stable at least up to the indicated passages for all related experiments (*SI Appendix*, Fig. S7).

Collectively, our results show that *B3GALT5*-KO cells cultured under 2iLAF conditions were converted to a naïve state having characteristics similar to naïve cells converted from WT hESCs in 5iLAF culture. These findings imply that loss of B3GALT5 led to dynamic changes in GSL profile, which could facilitate the generation of naïve pluripotency in hESCs, but did not affect pluripotency and ability for lineage-specific differentiation.

KO of *B3GALT5* Increases Intracellular Ca^{2+} Level. A recent study reported that control of intracellular Ca^{2+} is crucial for the exit from naïve pluripotency in mouse ESCs (31). However, the impact of Ca^{2+} on human naïve cells remains obscure. To investigate the role of Ca^{2+} homeostasis in human naïve pluripotency, intracellular Ca^{2+} levels were evaluated using a calcium indicator dye, Fluo-4 AM. As compared to primed H9 cells, intracellular Ca^{2+} was elevated markedly in naïve cells derived from either WT+5iLAF or KO+2iLAF and moderately in *B3GALT5*-KO cells (Fig. 4A). Besides, only WT cells treated with 5iLAF, but not 2iLAF, displayed higher intracellular Ca^{2+} content (*SI Appendix*, Fig. S8A). To assess the involvement of intracellular Ca^{2+} in the conversion of primed to naïve state, we examined effects of BAPTA-AM, an intracellular calcium chelator, during the transition process. Addition of BAPTA-AM to WT+5iLAF inhibited conversion of primed to naïve state in a dose-dependent manner, with loss of naïve-like colonies and naïve-markers at ≥7.5 μM (Fig. 4B). The similar results of intracellular Ca^{2+} level were also observed in WT and KO hESCs of HUES6 (*SI Appendix*, Fig. S8 *B* and *C*). These results demonstrate that intracellular calcium is required for primed to naïve conversion. In comparison, KO cells cultured in 2iLAF medium displayed more resistance to the inhibition of primed to naïve conversion by BAPTA-AM than the WT+5iLAF sample, requiring ≥10 μM to achieve complete block of naïve conversion. This was consistent with the finding that KO cells had higher level of intracellular Ca^{2+} than WT hESCs. Since Ca^{2+} is considered to be a guardian of naïve pluripotency (31), the increase in Ca^{2+} concentration may account for the intermediate state of *B3GALT5* KO during transition toward naïve pluripotency. These results lend further support that an increase in intracellular Ca^{2+} concentration is also important for human naïve pluripotency and implies that *B3GALT5* KO may facilitate the primed to naïve conversion through raising Ca^{2+} level intracellularly.

In conclusion, our studies characterize the dynamic changes in GSL profile and glycosyltransferase activities during the primed to naïve transition of pluripotency in hESCs. In addition, we demonstrate that the loss of a single glycosyltransferase, B3GALT5, leads to a shift of glycan expression from globo- (SSEA-3, SSEA-4, and Globo H) and lacto-(fucosyl-Lc4Cer) series to neolacto- (SSEA-1 and H type 2) series and increases intracellular Ca2+, which promotes the pluripotency transition. Thus, our results provide a new perspective in the understanding of human pluripotency transition, which can be mediated by B3GALT5 to facilitate the primed and naïve transition (Fig. 5).

Discussion

We previously reported that globo- and lacto-series GSLs, including SSEA-3, SSEA-4, Globo H, Gb4Cer/Lc4Cer, and fucosyl-Lc4Cer, are highly expressed in undifferentiated hESCs

and disappear upon differentiation of hESCs into embryoid bodies (18, 20). A recent report indicated that only SSEA-4⁻ cells after culture of hESCs in 5iLAF media possessed features characteristic of the naïve state (5). Using combined mAb and MS analysis, we showed that in addition to SSEA-4, there was loss of other globo- and lacto-series GSLs, originally expressed in primed-state cells, upon conversion to naïve pluripotency. These globo-series GSLs share the type 4 glycan (Galβ1–3GalNAc) derived from the precursor Gb4Cer by the addition of β1–3 galactose catalyzed by B3GALT5 (32). Moreover, the lacto-series GSL fucosyl-Lc4Cer (H type 1) was lost in naïve-state hESCs, since mAbs against H type 1 glycan (Fucα1–2Galβ1–3GlcNAc) stained only primed-state hESCs (18, 20). Furthermore, naïve hESCs in 5iLAF culture and *B3GALT5*-KO hESCs had a loss of TRA-1-60 and TRA-1-81, consistent with the report that both TRA-1-60 and TRA-1-81 recognize a specific type 1 chain epitope (26). Thus, the loss of globo (type 4)- and lacto (type 1)-series GSLs on the cell surface seems to be a general feature of naïve state and *B3GALT5*-KO hESCs.

In contrast, there was increased expression of the neolacto-series SSEA-1 and H type 2 antigen (type 2 family) in naïve state and *B3GALT5*-KO hESCs. The changes were accompanied by altered expression of several glycosyltransferases involved in GSL biosynthesis, particularly marked down-regulation of B3GALT5 in naïve-state cells. In GSL biosynthesis, ceramide is glucosylated in *cis*-Golgi to produce a precursor glucosylceramide (GlcCer), which is and then converted to lactosylceramines (LacCer, Gal-GlcCer) before further modification to yield globo-, lacto-, neolacto-, ganglio-, and asialo- series GSLs (Fig. 1D) (33, 34). B3GALT5 catalyzes the addition of β1–3 galactose to Gb4Cer/Lc3Cer and is responsible for the biosynthesis of both type 4 (Galβ1–3GalNAc) and type 1 (Galβ1–3 GlcNAc) glycan core structures in the globo-and lacto-series GSLs, respectively (19), which are abundantly expressed in primed hESCs. In *B3GALT5*-KO and naïve hESCs, the primed-state–associated expressions of globo- and lacto-series GSLs (type 4 and type 1 families) were lost. Interestingly, an obligatory increase in the expression of type 2 chain glycans (Galβ1–4 GlcNAc) was noted in naïve state and *B3GALT5*-KO cells, as indicated by the detection of SSEA-1 and H type 2 antigen in these cells. These results imply that B3GALT5 blockade may cause a shift to an alternative pathway with the addition of galactose via β1–4 linkage by β1,4-galactosyltransferases (B4GALTs), resulting in increased expression of the type 2 epitope family (35). Such dynamic changes in type 1 and 2 glycoconjugate families will need to be further investigated by MS/MS analysis, since their precursors, Lc4Cer and nLc4Cer, have the same molecular weight, yielding common molecular ions on MS analysis. Furthermore, as type 1 and 2 structures are also found in N- and O-linked glycans (19), it remains unclear whether *B3GALT5* KO leads to changes in glycosylation of proteins carrying these epitopes. Collectively, our data support the conclusion that B3GALT5 plays a major role in the appearance of these interesting antigens, resulting in a unique cell surface glycan pattern conducive for transition to the naïve state. Thus, B3GALT5 may be an important glycosyltransferase in governing different states of stem cell pluripotency.

SSEA-1 is known to be expressed in murine ESCs and early mouse embryos, but not hESCs. Previously, naïve hESCs derived directly from human inner cell mass or converted from the primed state were reported to lack SSEA-1 expression (6, 10). A recent study showed that SSEA-1 is expressed in naïve-like cells converted from human deciduous teeth dental pulp cell-derived induced pluripotent stem cells (36), consistent with our observation in hESCs with naïve features under 5iLAF conditions and *B3GALT5*-KO cells. As different protocols were used for conversion of primed hESCs to the naïve state (37), whether SSEA-1 is specifically expressed in human naïve cells will need further investigation. On the other hand, we observed that another type
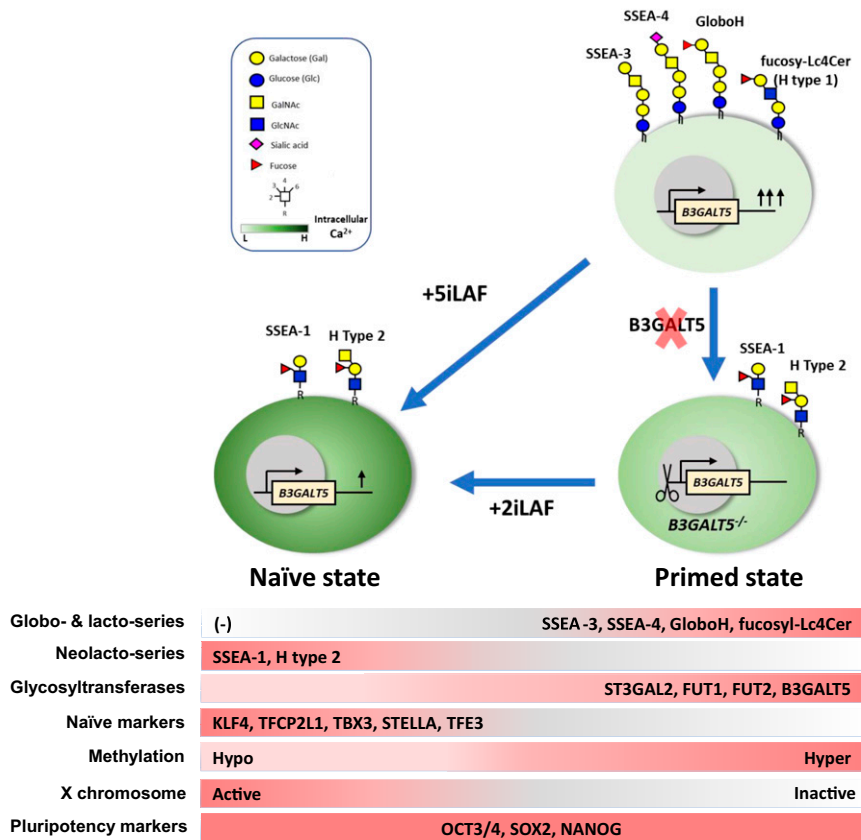
Fig. 5. Graphical illustration of the dynamic changes in GSLs and intracellular Ca^{2+} during transition of human ESCs from primed to naïve pluripotency.

2 family member, H type 2 antigen, is expressed in naïve and *B3GALT5*-KO hESCs. It will be of interest to determine whether high expression of SSEA-1, type 2 H antigen, or other unexplored neolacto-GSLs or glycoproteins containing a neolacto type 2 core chain contribute to the maintenance of human naïve pluripotency, and facilitate embryo implantation.

In addition to the loss of globo- and lacto-series GSLs, *B3GALT5* KO cells also displayed increased single-cell cloning efficiency and intracellular Ca^{2+}, similar to naïve-state cells, and retained the ability to form three germ layers in vitro and in vivo. Moreover, *B3GALT5*-KO hESCs displayed a naïve-like transcriptome and other hallmarks of the naïve state, such as global DNA hypomethylation and X chromosome reactivation upon 2iLAF culture. Our study not only demonstrated increased intracellular calcium in human naïve pluripotent cells as reported in mouse ESCs (31), but also uncovered an unexpected role of B3GALT5 in modulating intracellular calcium level. Emerging evidence supports that GSLs can function as a signal transducer in cellular differentiation and interaction (7, 38). Besides, FGF2-, TGF-β–, and Wnt-mediated signaling pathways, which are involved in pluripotency maintenance, have also been shown to modulate cytoplasmic calcium concentration (39). It is thus intriguing to speculate that KO of *B3GALT5* resulting in changes in GSLs or glycans may cooperate with factors such as 2i, LIF, or bFGF to increase cytoplasmic calcium, which facilitate the transition to the naïve state. However, detailed mechanism and regulatory pathways involved await further investigation.

Materials and Methods

See *SI Appendix, Supplementary Methods* for a detailed description of establishment of *B3GALT5* KO clones in hESCs, differentiation, MALDI-MS/MS-MS analysis for permethylated GSLs, and karyotype analysis.

hESC Lines and Culture Condition. H9 and HUES6 hESC lines were obtained from WiCell Research Institute (WA09), and Melton Lab, Harvard University, respectively. The hESCs aspect of the research was performed under a protocol approved by the Chang Gung Memorial Hospital Institutional Review Board Committee. Primed hESCs, were maintained in DMEM/F12, 20% Knockout Serum Replacement, 1% nonessential amino acids, 2 mM GlutaMAX, 50 U/mL and 50 μg/mL penicillin-streptomycin, 0.1 mM β-mercaptoethanol, and 4 ng/mL basic fibroblast growth factor (all from Gibco) on mitomycin C (10 μg/mL; Sigma-Aldrich) treated mouse embryonic fibroblasts (MEF) seeded at a density of 1 × 10^6 cells per well of six-well plates. Cells were passaged by 12- to 15-min incubation with Dispase (Stemcell Technologies) every 7 d (1:6 ratio). For feeder-free culture, primed hESCs were transferred onto Matrigel-coated plates (Corning) in the complete E8 medium (Gibco). Cells were passaged by 4-min incubation at room temperature with Cell Dissociation Buffer (Gibco) every 5 d (1:7 to 1:10 ratio). Only passages 20 to 30 post-E8 adaptations were used for all experiments described here.

Establishment of *B3GALT5* KO Clones in hESCs. *B3GALT5*-KO clones were developed by introducing a CRISPR/Cas9 vector containing *B3GAL5* guide sequences into H9 or HUES6 cells by transfection, as described in detail in *SI Appendix, Supplementary Methods*.

Generation of B3GALT5 Overexpression Cells. Full-length *B3GALT5* was amplified out of a human cDNA and inserted into the lentivirus-based expression vector pCDH-CMV-MCS-EF1α-copGFP (System Biosciences, #CD511B-1) generating pCDH-*B3GALT5*-GFP construct. Lentivirus were prepared according to the manufacturer's instructions. For overexpression of B3GALT5, KO cells were infected with vector only or pCDH-*B3GALT5*-GFP virus in the presence of polybrene, 8 μg/mL. Two days after infection, the stably transfected clones (KO+OE Ctrl-GFP or KO+OE *B3GALT5*-GFP) were selected by GFP.

Primed-State to Naïve-State Conversion. H9 cells were cultured under 5iLAF conditions following a published 5iLAF protocol (4, 8). Cells in a medium containing a 1:1 mixture of DMEM/F12 and Neurobasal, 1% N2 supplement,

1% B-27 supplement, 1% nonessential amino acids, 2 mM GlutaMAX, 50 U/mL and 50 μg/mL penicillin-streptomycin, 0.1 mM β-mercaptoethanol, 0.5% Knockout Serum Replacement (all from Gibco), 50 μg/mL BSA (Sigma-Aldrich), 20 ng/mL recombinant human LIF (Millipore), 20 ng/mL activin A (Peprotech), 8 ng/mL bFGF (Peprotech), and five inhibitors: 1 μM PD0325901 (Sigma-Aldrich), 1 μM IM-12 (Selleck Chemicals), 1 μM WH-4-023 (Tocris Ellisville), 0.5 μM SB590885 (Tocris Ellisville), and 10 μM Y-27632.

H9 cultured under 2iLAF conditions were maintained as previously described (8, 9) in a medium containing 1:1 mixture of DMEM/F12 and Neurobasal, 1% N2 supplement, 1% B-27 supplement, 1% nonessential amino acids, 2 mM GlutaMAX, 50 U/mL and 50 μg/mL penicillin-streptomycin, 0.1 mM β-mercaptoethanol, 0.5% Knockout Serum Replacement, 50 μg/mL BSA, 20 ng/mL recombinant human LIF, 20 ng/mL activin A, 8 ng/mL bFGF, and 2 inhibitors: 1 μM PD0325901 and CHIR99021 (Caymen). For primed-to-naïve conversion, cells were cultured in 5iLAF or 2iLAF condition for at least three passages but up to seven passages for all related experiments.

For the intracellular calcium experiment, cells were cotreated with/without BAPTA-AM (10 μM, ThermoFisher) under 5iLAF or 2iLAF conditions. Briefly, cells were seeded on an MEF layer at a density of 2.5×10^6 cells per well of 12-well plates. Cells were passaged by a 5-min incubation with TrypLE. For MS and qPCR analyses, naïve cells were detached by treatment with Cell Dissociation Reagent for 45 to 60 min, which allowed selective detachment of cell colonies from feeder cells.

Teratoma Formation. For teratoma formation, 1×10^6 *B3GALT5*-KO cells were prepared and resuspended in 50 μL of DMEM/F12 and mixed with 50 μL of Matrigel. These cells were used to inject immunocompromised NSG (NOD scidγ) mice. Each mouse received both subcutaneous and intramuscular injections. Tumors developed after 6 to 9 wk and were processed for histological analysis.

Cloning Efficiency Assay. The cloning assay has been described previously (40). Briefly, cells were prepared in octuplicate in a 96-well plate format for each treatment. Prior to the addition of cells, 100 μL of E8 media with 10 μM Y-27632 were loaded into each well. Cells were dissociated with Accutase for 5 to 10 min or until fully detached from the plate, neutralized with equal volumes of PBS, counted, washed, and then diluted to 250 cells/mL in the same media. Finally, a 100-μL suspension (25 cells) was added to each well. Media were changed every 2 d if not specified. After 3 to 4 d, colonies were stained with DAPI or Oct4 and counted.

Immunostaining. For immunofluorescence staining, cells grown on Matrigel-coated plate or MEF-coated plates were fixed with 4% (wt/vol) paraformaldehyde in PBS at room temperature for 10 min and washed three times with 1× PBS. Cells were permeabilized with 0.1% Triton X-100 (wt/vol) for 5 min. Then cells were incubated in blocking solution (0.1% Triton X-100 plus 2% donkey serum in 1× PBS) for 1 h. Primary antibodies were added into the blocking solution and incubated at 4 °C overnight. The next day, cells were washed three times with 1× PBS. Secondary antibodies conjugated to Alexa Fluor 488 or 555 (Thermo Fisher Scientific) were incubated for 1 h. For nuclear staining, cells were incubated with DAPI (Sigma-Aldrich) for 3 min. Images were taken using a Leica DMI6000 B (Leica Microsystems) or DMi8 microscope (Leica Microsystems). Primary antibodies are listed in *SI Appendix*, Table S1.

qRT-PCR. Total RNA was isolated using the RNeasy Mini RNA Isolation kit (Qiagen) and reverse-transcribed to cDNA by using a High-Capacity cDNA Reverse Transcription kit (ThermoFisher Scientific). The cDNA reaction was diluted 1:10 in ddH$_2$O and used in Fast SYBR Green real-time PCR reactions (ThermoFisher Scientific). All reactions were run in duplicate or triplicate on a QS7 machine (Applied BioSystems) according to the manufacturer's instructions. Values were normalized to ACTB, GAPDH, GUSB, or UBC, and then compared to control cells. Primer sequences are listed in *SI Appendix*, Table S2. For detection of glycosyltransferase genes, real-time PCR was performed using TaqMan Universal PCR Master Mix (ThermoFisher Scientific) and TaqMan gene-expression assays (ThermoFisher Scientific). The TaqMan Probes are listed in *SI Appendix*, Table S3.

RNA-Seq Method and Data Analysis.
Library preparation and sequencing. The purified RNA was used for the preparation of the sequencing library by TruSeq Stranded mRNA Library Prep Kit (Illumina) following the manufacturer's recommendations. Briefly, mRNA was purified from total RNA (1 μg) by oligo(dT)-coupled magnetic beads and fragmented into small pieces under elevated temperature. The first-strand cDNA was synthesized using reverse transcriptase and random primers. After

the generation of double-strand cDNA and adenylation on 3′ ends of DNA fragments, the adaptors were ligated and purified with AMPure XP system (Beckman Coulter). The quality of the libraries was assessed on the Agilent Bioanalyzer 2100 system and a real-time PCR system. The qualified libraries were then sequenced on an Illumina NovaSEq. 6000 platform with 150-bp paired-end reads generated by Genomics, BioSci & Tech Co.
Bioinformatics analysis. The bases with low quality and sequences from adapters in raw data were removed using the program Trimmomatic (v0.39). The filtered reads were aligned to the reference genomes (hg19) using Bowtie2 (v2.3.4.1). A user-friendly software RSEM (v1.2.28) was applied for the quantification of the transcript abundance. DEGs were identified by EBSeq (v1.16.0). The PCA analysis and heatmap were generated by the ClustVis (https://biit.cs.ut.ee/clustvis/) based on DEGs between primed and naïve hESCs.
Allelic expression analysis of X-linked transcript. The RNA-seq reads were removed adapter and primer sequences, and trimmed to retain high-quality data (Q20). The sequence reads were filtered (>100 reads), aligned to human reference genome hg19. Informative SNPs within X-linked genes of the H9 cells (30) were used to classify the transcript as monoallelic or biallelic. Briefly, genome reads which corresponding to reads carrying either of two alleles, were quantified with BCFtools Mpileup (v1.9). Transcripts were classified as biallelic when at least 30% of reads originated from the second allele.

RNA-FISH. Cells were collected and resuspended in hypotonic 0.075 M potassium chloride for 30 min at 37 °C followed with fixed in methanol/glacial acetic acid 3:1. The fixed cells were dropped on the slide and air-dried. The slides were denatured for 5 min at 72 °C and hybridized overnight with labeled probes in FISH hybridization buffer at 37 °C. After cytology Stringency wash buffer SSC (Zyovision) wash for 2 min at 70 °C and cytology wash buffer SSC (Zyovision) wash for 1 min at room temperature, slides were mounted in DAPI/DuraTect-Solution (Zyovision). The Green-dUTP labeled FISH probe for HUWE1 (RP11-975N19) was purchased from Empire Genomics. Images were acquired using a Leica DFC495 microscope. Expression of HUWE1 was manually counted in more than 100 cells per cell line.

Bisulfite Sequencing and Analysis. Genomic DNA was extracted using the Gentra Puregene Cell Kit (Qiagen) and quantified using a NanoDrop ND-2000 Spectrophotometer (ThermoFisher Scientific). Construction of DNA libraries and subsequent DNA sequencing were performed by the Genomic Medicine Core Laboratory, Linkou, Chang Gung Memorial Hospital. Briefly, bisulfite sequencing libraries were prepared using the Truseq methyl capture EPIC library kit (Illumina). Unmethylated λ-phage DNA was spiked in at input DNA quantity to determine conversion efficiency, which was 99% for all libraries. Libraries were sequenced in 125-bp paired-end on Illumina HiSEq. 4000 (Illumina). Sequencing reads were processed to remove the first six bases, adapter sequences, and poor-quality reads; the remaining sequences were mapped to human genome build GRCh37/hg19 using CLC Genomics Workbench v11.0.0 (Qiagen). The CpG methylation calls were extracted and analyzed using MATLAB software. Global comparison, correlation and PCA analysis of CpG methylation between samples was calculated by MATLAB software.

Intracellular Calcium Measurement and Visualization. WT and KO cells were seeded in Matrigel-coated μ-Slide 8 well (Ibidi). Cells were loaded with 5 mM Fluo-4 AM (ThermoFisher Scientific) in Tyrode's solution for 30 min, and washed twice with PBS to remove the extracellular dye. Probenecid (2.5 mM) was added to both the loading medium and the washing solution to prevent dye leakage. Ca^{2+} imaging was conducted using a fluorescent microscope (Leica DMI6000).

Quantification and Statistical Analysis. Data are presented as the mean ± SEM or mean ± SD using GraphPad Software Prism 6. Statistical significance was determined by Student's *t* tests. Values of $P \leq 0.05$ were considered to be statistically significant.

Data Availability. The RNA-seq and bisulfite-sequencing datasets used for this study have been deposited in the Gene Expression Omnibus (GEO) database, https://www.ncbi.nlm.nih.gov/geo (accession nos. GSE156515 and GSE134193).

1. J. Nichols, A. Smith, Naive and primed pluripotent states. *Cell Stem Cell* **4**, 487–492 (2009).

2. L. Weinberger, M. Ayyash, N. Novershtern, J. H. Hanna, Dynamic stem cell states: Naive to primed pluripotency in rodents and humans. *Nat. Rev. Mol. Cell Biol.* **17**, 155–169 (2016).

3. A. Deb, A. Sarkar, Z. Ghosh, Dissecting the variation in transcriptional circuits between naive and primed pluripotent states. *FEBS Lett.* **591**, 2362–2375 (2017).

4. T. W. Theunissen et al., Molecular criteria for defining the naive human pluripotent state. *Cell Stem Cell* **19**, 502–515 (2016).

5. W. A. Pastor et al., Naive human pluripotent cells feature a methylation landscape devoid of blastocyst or germline memory. *Cell Stem Cell* **18**, 323–329 (2016).

6. A. J. Collier et al., Comprehensive cell surface protein profiling identifies specific markers of human naive and primed pluripotent states. *Cell Stem Cell* **20**, 874–890.e7 (2017).

7. S. Nishihara, Glycans define the stemness of naïve and primed pluripotent stem cells. *Glycoconj. J.* **34**, 737–747 (2017).

8. T. W. Theunissen et al., Systematic identification of culture conditions for induction and maintenance of naive human pluripotency. *Cell Stem Cell* **15**, 524–526 (2014).

9. Y. Takashima et al., Resetting transcription factor control circuitry toward ground-state pluripotency in human. *Cell* **158**, 1254–1269 (2014).

10. O. Gafni et al., Derivation of novel human ground state naive pluripotent stem cells. *Nature* **504**, 282–286 (2013).

11. H. Qin et al., YAP induces human naive pluripotency. *Cell Rep.* **14**, 2301–2312 (2016).

12. K. Huang, T. Maruyama, G. Fan, The naive state of human pluripotent stem cells: A synthesis of stem cell and preimplantation embryo transcriptome analyses. *Cell Stem Cell* **15**, 410–415 (2014).

13. T. Muramatsu, H. Muramatsu, Carbohydrate antigens expressed on stem cells and early embryonic cells. *Glycoconj. J.* **21**, 41–45 (2004).

14. S. I. Hakomori, Glycosynaptic microdomains controlling tumor cell phenotype through alteration of cell growth, adhesion, and motility. *FEBS Lett.* **584**, 1901–1906 (2010).

15. S. I. Hakomori, Structure and function of glycosphingolipids and sphingolipids: Recollections and future trends. *Biochim. Biophys. Acta* **1780**, 325–346 (2008).

16. J. C. Manimala, T. A. Roach, Z. Li, J. C. Gildersleeve, High-throughput carbohydrate microarray profiling of 27 antibodies demonstrates widespread specificity problems. *Glycobiology* **17**, 17C–23C (2007).

17. A. Barone et al., Structural complexity of non-acid glycosphingolipids in human embryonic stem cells grown under feeder-free conditions. *J. Biol. Chem.* **288**, 10035–10050 (2013).

18. Y. J. Liang et al., Switching of the core structures of glycosphingolipids from globo- and lacto- to ganglio-series upon human embryonic stem cell differentiation. *Proc. Natl. Acad. Sci. U.S.A.* **107**, 22564–22569 (2010).

19. M. Y. Ho, A. L. Yu, J. Yu, Glycosphingolipid dynamics in human embryonic stem cell and cancer: Their characterization and biomedical implications. *Glycoconj. J.* **34**, 765–777 (2017).

20. Y. J. Liang et al., Changes in glycosphingolipid composition during differentiation of human embryonic stem cells to ectodermal or endodermal lineages. *Stem Cells* **29**, 1995–2004 (2011).

21. B. Di Stefano et al., Reduced MEK inhibition preserves genomic stability in naive human embryonic stem cells. *Nat. Methods* **15**, 732–740 (2018).

22. T. Messmer et al., Transcriptional heterogeneity in naive and primed human pluripotent stem cells at single-cell resolution. *Cell Rep.* **26**, 815–824.e4 (2019).

23. H. Sperber et al., The metabolome regulates the epigenetic landscape during naive-to-primed human embryonic stem cell transition. *Nat. Cell Biol.* **17**, 1523–1535 (2015).

24. Y. S. Chan et al., Induction of a human pluripotent state with distinct regulatory circuitry that resembles preimplantation epiblast. *Cell Stem Cell* **13**, 663–675 (2013).

25. S. Isshiki et al., Cloning, expression, and characterization of a novel UDP-galactose: beta-N-acetylglucosamine beta1,3-galactosyltransferase (beta3Gal-T5) responsible for synthesis of type 1 chain in colorectal and pancreatic epithelia and tumor cells derived therefrom. *J. Biol. Chem.* **274**, 12499–12507 (1999).

26. S. Natunen et al., The binding specificity of the marker antibodies Tra-1-60 and Tra-1-81 reveals a novel pluripotency-associated type 1 lactosamine epitope. *Glycobiology* **21**, 1125–1130 (2011).

27. J. Hanna et al., Human embryonic stem cells with biological and epigenetic characteristics similar to those of mouse ESCs. *Proc. Natl. Acad. Sci. U.S.A.* **107**, 9222–9227 (2010).

28. X. Liu et al., Comprehensive characterization of distinct states of human naive pluripotency generated by reprogramming. *Nat. Methods* **14**, 1055–1062 (2017).

29. A. Sahakyan et al., Human naive pluripotent stem cells model X chromosome dampening and X inactivation. *Cell Stem Cell* **20**, 87–101 (2017).

30. C. Vallot et al., Erosion of X Chromosome inactivation in human pluripotent cells initiates with XACT coating and depends on a specific heterochromatin landscape. *Cell Stem Cell* **16**, 533–546 (2015).

31. M. S. MacDougall, R. Clarke, B. J. Merrill, Intracellular Ca(2+) homeostasis and nuclear export mediate exit from naive pluripotency. *Cell Stem Cell* **25**, 210–224.e6 (2019).

32. D. Zhou, T. R. Henion, F. B. Jungalwala, E. G. Berger, T. Hennet, The beta 1,3-galactosyltransferase beta 3GalT-V is a stage-specific embryonic antigen-3 (SSEA-3) synthase. *J. Biol. Chem.* **275**, 22631–22634 (2000).

33. L. Cooling, Blood groups in infection and host susceptibility. *Clin. Microbiol. Rev.* **28**, 801–870 (2015).

34. D. Russo, L. Capolupo, J. S. Loomba, L. Sticco, G. D'Angelo, Glycosphingolipid metabolism in cell fate specification. *J. Cell Sci.* **131**, jcs219204 (2018).

35. M. Amado, R. Almeida, T. Schwientek, H. Clausen, Identification and characterization of large galactosyltransferase gene families: Galactosyltransferases for all functions. *Biochim. Biophys. Acta* **1473**, 35–53 (1999).

36. E. Inada et al., Increased expression of cell surface SSEA-1 is closely associated with naïve-like conversion from human deciduous teeth dental pulp cells-derived iPS cells. *Int. J. Mol. Sci.* **20**, E1651 (2019).

37. O. Trusler, Z. Huang, J. Goodwin, A. L. Laslett, Cell surface markers for the identification and study of human naive pluripotent stem cells. *Stem Cell Res. (Amst.)* **26**, 36–43 (2018).

38. T. Zhang, A. A. de Waard, M. Wuhrer, R. M. Spaapen, The role of glycosphingolipids in immune cell functions. *Front. Immunol.* **10**, 90 (2019).

39. Á. Apáti, T. Berecz, B. Sarkadi, Calcium signaling in human pluripotent stem cells. *Cell Calcium* **59**, 117–123 (2016).

40. G. Chen et al., Chemically defined conditions for human iPSC derivation and culture. *Nat. Methods* **8**, 424–429 (2011).